

RSC Advances



This is an *Accepted Manuscript*, which has been through the Royal Society of Chemistry peer review process and has been accepted for publication.

Accepted Manuscripts are published online shortly after acceptance, before technical editing, formatting and proof reading. Using this free service, authors can make their results available to the community, in citable form, before we publish the edited article. This *Accepted Manuscript* will be replaced by the edited, formatted and paginated article as soon as this is available.

You can find more information about *Accepted Manuscripts* in the [Information for Authors](#).

Please note that technical editing may introduce minor changes to the text and/or graphics, which may alter content. The journal's standard [Terms & Conditions](#) and the [Ethical guidelines](#) still apply. In no event shall the Royal Society of Chemistry be held responsible for any errors or omissions in this *Accepted Manuscript* or any consequences arising from the use of any information it contains.

Cite this: DOI: 10.1039/c0xx00000x

www.rsc.org/xxxxxx

ARTICLE TYPE

Tailoring impact behavior of polyamide 6 ternary blends via hierarchical core-shell structure in situ formed in melt mixing

Rui Dou^a, Chao Shen^a, Bo Yin^{*a}, Ming-bo Yang^a and Bang-hu Xie^a^a College of Polymer Science and Engineering, Sichuan University, State Key Laboratory of Polymer Materials Engineering, Chengdu, 610065 Sichuan, China. E-mail: yinbo@scu.edu.cn

Received (in XXX, XXX) Xth XXXXXXXXX 20XX, Accepted Xth XXXXXXXXX 20XX

DOI: 10.1039/b000000x

PA6-based ternary blends were prepared by melt blending of HDPE-g-MA and EPDM rubber, in which EPDM with a low and high viscosity was respectively selected to construct different core-shell morphology. And the core-shell morphology evolution was subsequently controlled via quiescent melt annealing. The relationship between the hierarchical core-shell structure and impact behaviors were studied systematically. Righting after extrusion, the dispersed domains in low viscosity EPDM blends displayed a single core-shell structure while a multi-core structure with multiple HDPE-g-MA particles within EPDM2 phase formed in high viscosity EPDM blends. During annealing, the lower viscosity EPDM blends displayed a core-shell size coarsening phenomenon without core-shell morphological type changed. However, for higher viscosity EPDM blends, the initial multi-core structure evolved into a complete EPDM single-core structure after annealing. The notched Izod impact test indicated that the ternary blends with a multi-core structure had much higher impact toughness than that of other blends. The crack-initiation pattern, impact fractured surface and cross-section of the impact surface tests have been performed to study the impact mechanism. The results indicated that HDPE-g-MA particles within multi core-shell structure could both enhance the core-shell particles strength and enlarge interfacial areas which avoided the rupture and debonding of multi-core particles. Also these core-shell particles could prevent propagation of the crack effectively, thus obtained higher notched Izod impact strength.

I. Introduction

Polymer blending is one of the most important ways of achieving a desirable combination of properties which are often absent in pure polymers.¹⁻⁵ As well, melt-blending allows for the generation of complex micro-structured multi-component blends. Also it is well known that the phase morphology is generally controlled not only by thermodynamic factors (interfacial tension, compatibility, composition ratio etc.⁶⁻⁹) but also by kinetic factors (viscosity ratio, mixing sequent, mixing of temperature, screw speed etc.^{10, 11-13}). More importantly, the properties of polymer blends are largely depend on its phase morphology.^{1, 5, 10, 14-16} Therefore, to achieve the best combination of mechanical properties, the key is to control the phase morphology of polymer blends.

As is well known, the excellent toughness of high impact polystyrene (HIPS) depends on the formation of particular salami-like microstructure.¹⁷ The satisfactory toughening effect of poly (lactic acid) (PLA) often depends on the balance between interfacial compatibilization and crosslinking of the elastomer.¹⁸ Moreover, DR Paul et al. found that the rubber particle size,^{19, 20} rubber type²¹ and crystallization behavior²² played a significant role on the mechanical properties of rubber-toughened polymer, which made significant contributions in the field of polymer toughening.

Recently, because multi-component polymer blends can demonstrate a wide variety of micro-structured morphologies

with multiple interfaces present, more attention has been paid to the ternary polymer blends and many researchers have focus on optimizing the mechanical properties of blends containing core-shell microstructure dispersed in a polymer matrix.^{10, 23-25} Luzinov et al.²⁵ discussed the morphology and mechanical properties of ternary blends consisting of polystyrene matrix and polyolefin/styrene butadiene rubber core-shell dispersed phases. The ultimate mechanical properties of the blends showed some dependence on the stiffness of the PO core according to their conclusion. Fu et al.²⁴ succeed to obtain a high toughness PP/EPDM/SiO₂ blends via the formation of EPDM/SiO₂ core-shell structure. The toughening mechanism they believed was that SiO₂ agglomerate around EPDM increased the effective size of the rubber particles, making the stress fields around SiO₂ particles served as a bridge between two neighboring rubber particles which resulting a higher impact strength. Zhuo Ke et al.²³ studied the mechanical properties and the morphologies for ternary blends of a core-shell structure with a low density polyethylene core and an elastic polybutadiene shell in Polyamide 6 (PA6) matrix. For blend with 90 wt % PA and 10 wt % core-shell toughener, they found that there was only a 10 % loss in modulus but a 10-fold increase in impact toughness compared to neat PA6.

However, majority previous works place more emphasis on the performance improvement for multi-components blends, toughening mechanism responsible for the core-shell structure toughened blends has not been comprehensively established so far. Concerning the toughening mechanism, one of the most

important findings in polymer-toughening is known as the critical matrix ligament thickness (t_c) theory, which is developed by Wu after an investigation on nylon 6/EPDM blends.²⁶ They found only when the matrix ligament thickness (t) is smaller than t_c could the shear yielding of matrix ligament exist and does a sharp brittle–ductile transition of blends occur. Over the years, theoretical^{27–29} and experimental^{30,31} studies show that the role of rubber on toughening of semi-crystalline polymers is mostly related to the cavitation of the filler. The high dilative stresses produced in front of a growing crack induce the formation of voids in or around the rubber particles. As a result, cavitated particles act then as stress concentrators around which the matrix can deform plastically and thus absorb much fracture energy.

In our previous work, Li et al.^{10,32} firstly discovered that the HDPE/EPDM-g-MA core/shell structure showed the outstanding superiority on the toughness improvement of PA6-based ternary blends compared to the rubber toughed PA6/EPDM blends. Also the difference of toughening mechanism between pure rubber particles in PA6/EPDM-g-MA binary blends and core-shell particles in PA6/EPDM-g-MA/HDPE ternary blends was discussed. They found that the fibrillation of core-shell particles in PA6/EPDM-g-MA/HDPE ternary blends, as “Particles Bridge”, can absorb fracture impact energy and sustain a higher stress so as to obtain the effect of strain hardening and prevent micro-crack further propagating. This result may have provided us with new insights into the toughening mechanism of ternary blend containing core-shell morphology.

However, what is still unknown is how core-shell structure is governed by the thermodynamic factors and kinetic factors and how the resulting changes in the microstructure of core-shell particles size and type influences impact behavior of the final blends. Up to now, the effect of core-shell particle size and type on impact behavior of PA6 blends and the associated toughening mechanism in relation to the micromechanical deformation process have been still not completely understood. With this aim in mind, in this study two EPDM with different viscosity were respectively employed in the ternary blends system to construct different core-shell morphology and the core-shell morphology evolution was subsequently controlled via quiescent melt annealing. The relation between hierarchical core-shell morphology and impact behavior of ternary blends was studied. Meanwhile, the mechanisms responsible for the changeable toughness of PA6/HDPE-g-MA/EPDM ternary blends with different core-shell morphology were comprehensively explored through DSC, OM and SEM tests.

II. Experimental section

Materials

Polyamide 6 (PA6), grade AKULON F136-C, was supplied by DSM, Netherland. Maleic anhydride grafted high density polyethylene (HDPE-g-MA), with the trademark TRD-100H was from Yizheng Siruida Plastic Company Ltd, China, had been grafted with 0.7 wt % maleic anhydride group. Two ethylene-propylene-diene monomers with different viscosity were used. EPDM 4770P (EPDM1) and EPDM 4725P (EPDM2) were both purchased from Dow. The properties of raw materials are listed in Table 1.

Sample Preparation

PA6 was dried in a vacuum oven for 24 h at 80°C before blending to minimize the effects of moisture. Ternary blends of PA6/HDPE-g-MA/EPDM1 (PHE1) and PA6/HDPE-g-MA/EPDM2 (PHE2), 70/15/15 based on weight fractions was prepared by adding the raw materials simultaneously into the feed cylinder and melt blended using a co-rotating twin-screw extruder

(Leistritz ZSE-18) with a screw diameter of 30.8 mm and an L/D ratio of 40. The screw speed was set at 150 rpm and the melt-zone temperatures were set to be 250 °C. The average shear rate was estimated to be $\dot{\gamma}=508.1 \text{ s}^{-1}$ based on the type of extruder. The extrudate was then quenched in cold water and pelletized. After drying to remove the moisture for 12 h under vacuum at 80 °C, the pellets were molded to sheets and bars at 250 °C in a press under a pressure of 10 MPa for 3 min, and were followed annealed at 250 °C with pressure for 0min, 10min, 20min, 40min and 60min, respectively, and then were cooled in the ambient air. In order to minimize the effect of degradation, the annealing test was conducted under a nitrogen atmosphere. The sheet was used for morphology observation and the bars with dimension of 78 mm × 10 mm × 4 mm (length × width × thickness) were used for notched Izod impact testing after machining notches (notch depth=2.0±0.1 mm). Then all the samples were kept at 23 °C for at least 48 h before testing. The as-obtained samples were labeled according to the blends components and annealing time. For example, the sample of PHE1-1 represented the PA6/HDPE-g-MA/EPDM1 blends after 10min melt annealing. The two different blends annealing 0min were labeled as PHE1-0 and PHE2-0, respectively.

Interfacial Tension Measurement

Several methods can be used to evaluate the interfacial tension between molten polymers.³³ In our previous work, the interfacial tensions were calculated by Wu’s equation.³⁴ However, it should be pointed that Wu’s equation was improper to evaluate the interfacial tension for polymer pairs involving PA6 and maleic anhydride grafted copolymers (such as HDPE-g-MA in this paper) because the reaction between the carboxyl group in maleic anhydride of HDPE-g-MA and the amino end group of PA6 could reduce the interfacial tension of the two phases. Therefore, the interfacial tension for the pairs of polymers in this study was determined using the rheological behavior of their respective blend. The data were analyzed using Gramespasher and Meissner’s³⁵ analyses following the procedures reported elsewhere.^{36–38} The results concerning the interfacial tensions are listed in Table 2.

These interfacial tension data used to calculate the spreading coefficients are listed in Table 3. For ternary blends of PA6/HDPE-g-MA/EPDM1 and PA6/HDPE-g-MA/EPDM2 blends, it is predicted that both EPDM1 and EPDM2 phase should be completely engulfed by the HDPE-g-MA dispersed phase.

Rheological Measurement

Steady-shear viscosity measurements of homopolymers were carried out using a RH7 high press capillary rheometer (Rohlin, England) under a temperature of 250 °C in a shear rate range from 20–2000s⁻¹. The measured shear viscosities of homopolymers are shown in Fig. 1.

Optical microscope (OM) observation

In order to examine the crack initiation stage, an arrested crack in the specimen was produced with an Izod impact tester. In detail, the pendulum was raised at an angle of 45 °C from the vertical and then released to hit the specimen. With appropriately chosen impact energy of about 1 J, the specimen was not broken into two halves, and the propagating crack stopped in the interior of the specimen. The slices with a thickness of 30 μm were cut along the crack propagation direction but perpendicular to the fracture surface. The morphologies of these thin sections were examined using Olympus BX51 polarizing optical microscopy (Olympus Co.,Tokyo, Japan) under both bright field and crossed-polar conditions.

Table 1 Polymer characteristics.

Polymers	Density at 25°C (g/cm ³)	$\eta_0 \times 10^{-3}$ (Pa.s) at 250 °C	Ethylene (wt %) ASTM D 3900	ENB (wt %) ASTM D 6047
PA6	1.13	2.0	-	-
HDPE-g-MA	0.93	15.0	-	-
EPDM1	0.88	1.5	70	4.9
EPDM2	0.88	14.2	70	4.9

η_0 : zero shear viscosity.

Table 2 Interfacial tension for polymer pairs at 250 °C.

Polymer pairs	Interfacial tension (mN/m)
PA6/HDPE-g-MA	0.7
PA6/EPDM1	11.7
EPDM1/HDPE-g-MA	0.7
PA6/EPDM2	21.9
EPDM2/HDPE-g-MA	1.7

Table 3 Spreading coefficients for the ternary PA6/HDPE-g-MA/EPDM1 and PA6/HDPE-g-MA/EPDM2 systems at 250 °C.

	Spreading coefficient (mN/m)
λ (HDPE-g-MA/EPDM1)	10.3
λ (HDPE-g-MA/EPDM2)	19.5

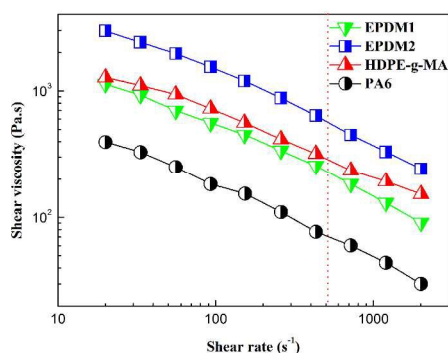


Fig. 1 Shear viscosity as a function of shear rate at 250 °C for EPDM1, EPDM2, HDPE-g-MA and PA6. The dashed lines represent the average shear rate during mixing.

Morphology Characterization

A JEOL JSM-5900LV scanning electron microscopy (SEM, JEOL, Japan) at a 20 kV accelerating voltage was used to observe the phase morphology of the blends. The samples were cryo-fractured in liquid nitrogen and the fractured surfaces were sputtered with gold before observation. Moreover, a transmission electron microscope (TEM) (Model: FEI-Tecnaï G2F20, USA) was also used to reveal the phase morphology of ternary blends. Ultra-thin sections having minimum thickness of 60 nm were cut using an ultra-microtome (Model: Leica-EM FC6, German) under the condition of sample temperature -80 °C. The sections were stained with OsO₄ for 10 min in order to enhance contrast.

Quantitative analysis of the dispersed morphology was performed using image analysis of Image-Pro Plus 6. At least 300 dispersed domains were measured to estimate number-average diameter (d_n) for each sample. Corrections to the particles size were performed using Schwartz–Saltykov method.³⁹

Characterization of crystal structure

The thermal analysis of the samples was conducted using a TA Q20 differential scanning calorimeter (New Castle, U.S.A.), calibrated by indium. Samples of about 5 mg were heated to 250 °C at a rate of 10 °C/min under a nitrogen atmosphere. Moreover heating curves were recorded for analysis. The degree of crystallinity was calculated from heat of fusion using 190 J/g

as the heat of fusion of 100% crystalline PA6.⁴⁰

Mechanical tests

The Izod notched impact strength of the specimens was measured with a VJ-40 Izod machine according to ASTM D256-04. At least seven specimens were tested and the average values were reported.

III. Results and discussion

3.1 Morphology of PA6/HDPE-g-MA/EPDM1 and PA6/HDPE-g-MA/EPDM2 blends after immediately extruding.

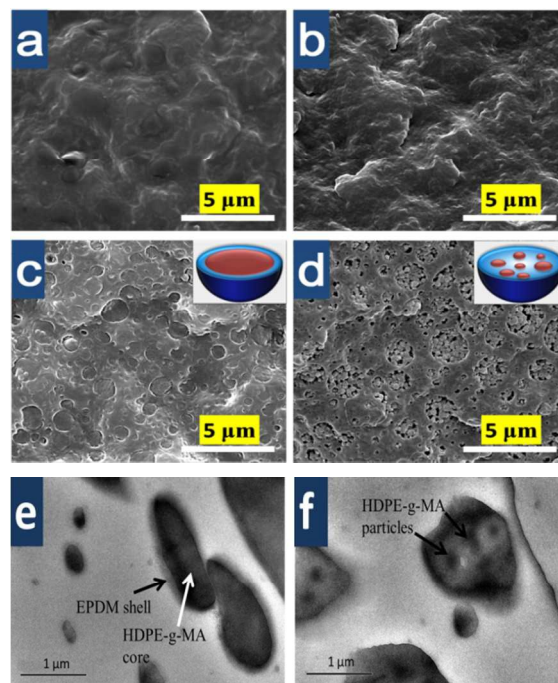


Fig. 2 Micrographs of cryo-fractured surface morphology of PA6/HDPE-g-MA/EPDM system for both EPDM materials after melt blending. (a, c and e) PHE1, (b, d and f) PHE2. (SEM photos for Fig. c and d with EPDM phase etched by xylene, and TEM photos for Fig. e and f of PHE1 and PHE2 blend with stained by OsO₄).

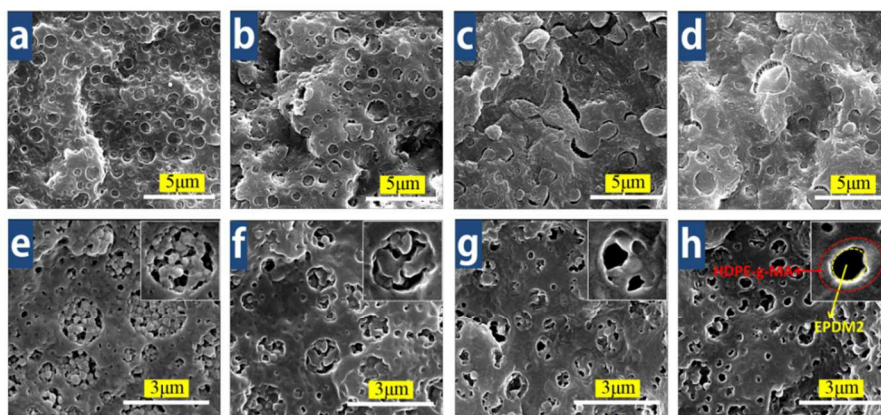


Fig. 3 SEM micrograph of ternary PA6/HDPE-g-MA/EPDM (70/15/15 wt%) system after (a) and (e) 0 min of annealing at 250 °C for EPDM1 and EPDM2 respectively; (b) and (f) 10 min for EPDM1 and EPDM2 respectively; (c) and (g) 40 min for EPDM1 and EPDM2 respectively; (d) and (h) 60 min for EPDM1 and EPDM2 respectively. (EPDM phase was etched by xylene)

Fig. 2 shows the phase morphology of PA6/HDPE-g-MA/EPDM for the EPDM1 and EPDM2 right after extruding. The interface between dispersion phase and PA6 matrix is very obscure both in the two blend system (seen in **Fig. 2a and b**). This is attributed to the reaction between the carboxyl group in maleic anhydride of HDPE-g-MA and the amino end group of PA6,⁴¹ which lead to a good compatibility between PA6 and HDPE-g-MA. In addition, because of the presence of ethylene chain segment in EPDM, HDPE-g-MA and EPDM is semimiscible, therefore the phase interface between HDPE-g-MA and EPDM was very indistinct. Combining the micrographs viewed from **Fig. 2c and d**, the phase morphology is great different between PA6/HDPE-g-MA/EPDM1 and PA6/HDPE-g-MA/EPDM2 blends. Typical single core-shell morphology with HDPE-g-MA phase encapsulated by EPDM1 was observed in the PA6/HDPE-g-MA/EPDM1 blends, while multi-core morphology with HDPE-g-MA particles within EPDM2 phase was found in the PA6/HDPE-g-MA/EPDM2 blends. Additionally, the formation of core-shell structure can also be confirmed by TEM, the dark cores in **Fig. 2e** were believed to be the HDPE-g-MA phase, and the encapsulated shell was EPDM1 phase. **Fig. 2d** of PHE2 ternary blends displayed “salami”-like substructure (multi-core structure), the dark inner inclusions HDPE-g-MA phase resided in the gray EPDM2 dispersed phase domains. The results cannot be explained through interfacial tension theory (shown in **Table 3**). Based on the results reported by Sundararaj *et al.*,^{42, 43} they assigned this phenomenon to a difference in softening temperature between both components. The lower melting component will always first encapsulate the higher melting component to form the matrix phase. In our present study, the formation of HDPE-g-MA phase encapsulated by both EPDM1 and EPDM2 can be attributed to a lower softening temperature of EPDM compared with HDPE-g-MA.

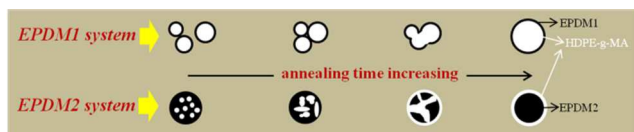


Fig. 4 A sketch showing core-shell morphology evolution of PHE1 and PHE2 blends during annealing.

Considering the different core-shell droplets type seen from **Fig.**

2c and d, it seems that the viscosity difference of EPDM1 and EPDM2 plays a crucial role on the formation of phase morphology. **Fig. 1** clearly demonstrates that EPDM2 has a higher shear viscosity than that of EPDM1 during melt mixing. And based on the theory of viscosity ratio, highly viscous matrices enhance droplet break-up due to their efficient shear stress transfer towards the dispersed phase and the higher dispersive forces acting on it; low viscous matrices often act as a lubricant for the dispersed phase reducing droplet break-up. Therefore, EPDM2 can transfer higher shear stresses to make HDPE-g-MA broke into small particles forming multi-core morphology compared with EPDM1. In the subsequent extrusion, the HDPE-g-MA subinclusions were immobilized by the highly viscous EPDM2 phase. The immobilization of HDPE subinclusions in the EPDM2 shell is also encouraged by the relatively low HDPE/EPDM-g-MA interfacial tension (shown in **Table 2**), this is also consistent with the results obtained by Favis.⁴⁴

3.2 Morphology evolution during quiescent annealing.

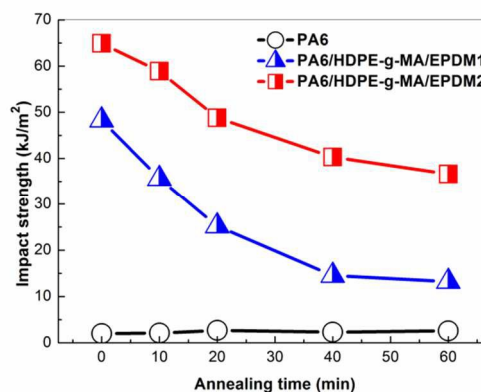


Fig. 5 Notched impact strength of different samples.

The morphology of both PHE1 and PHE2 after immediately extruding does not consistent with its thermodynamic equilibrium morphology. Therefore, quiescent melt annealing test was carried out. **Fig. 3** shows the evolution of the microstructure during annealing. Overall, many interesting features can be noticed from **Fig. 3**. The first observed phenomenon is an unchanged HDPE-g-MA/EPDM1 core-shell type during annealing for PA6/HDPE-g-MA/EPDM1 blend system. Only the dispersed phase enlarges continuously and gradually with annealing time. At the beginning, the average dispersed domain size is 0.49 μm. After undergoing

60min annealing, the droplets size increases to 0.90 μm . This phase coarsening behavior during annealing has been reported by many other researches.⁴⁵⁻⁴⁸ For the ternary blend of EPDM2 system seen through Fig. 3e-h, with annealing time increasing, HDPE-g-MA subinclusions tend to coarsen and migrate to the PA6/EPDM2 interface. After 40 min of quiescent annealing, most HDPE-g-MA phase has migrated to the PA6 matrix boundary (seen in Fig. 3g) before inverting to an almost complete HDPE-g-MA/EPDM2 shell/core structure (EPDM2 phase located within the HDPE-g-MA region) after 60 min (shown in Fig. 3h). Meanwhile, the composite droplets size decreases from 0.54 μm to 0.40 μm with annealing time. For EPDM2 system, the diameter decrease of composite droplets is likely caused by the reduction of the interfacial tension as well as the volume relaxation of dispersed phase during melt annealing.

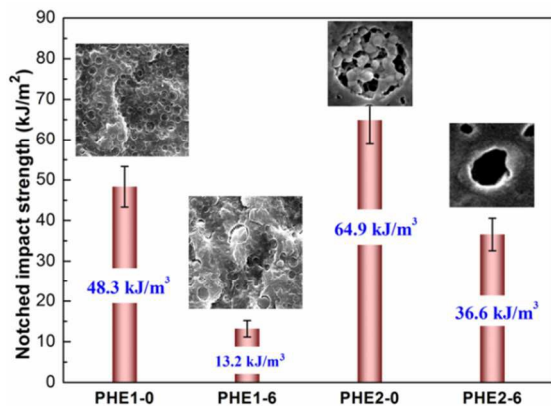


Fig. 6 Notched impact strength of different samples with various core-shell morphology.

Finally, a better understanding of Fig. 3 for the morphology evolution of PA6/HDPE-g-MA/EPDM blend system during annealing is summarized schematically in Fig. 4. The EPDM1 system displayed a size coarsening phenomenon of dispersed phase without core-shell morphological type changed during annealing. However, for EPDM2 system, the initial HDPE-g-MA multi-core morphology evolved into a complete EPDM2 single-core structure after annealing. Based on the results of morphology evolution, the next part will be focused on the understanding of structure-property relationship for both the two systems.

3.3 The notched impact strength

The impact property of the blends is exhibited in Fig. 5. Impact strength of PA6 keeps almost constant with annealing time. The increase of annealing time could reduce the toughness of the EPDM1 and EPDM2 ternary system markedly, and a ductile-brittle transition behavior could be noticed. But interestingly, impact strength of the EPDM2 system samples displays a higher value than that of the EPDM1 system samples during the whole annealing process. It is believed that the different core-shell microstructure between PA6/HDPE-g-MA/EPDM1 and PA6/HDPE-g-MA/EPDM2 blends during annealing is responsible for this phenomenon. And to our best knowledge, the relationship between core-shell morphology and toughness has never been comprehensively studied before. Here, seen from Fig. 6 we choose four typical samples with different core-shell microstructure (small rubber shell particle, larger rubber shell particle, multi-core particle and HDPE-g-MA shell particle) as our research focus to investigate the toughening mechanism in the subsequent section.

3.4 Toughening mechanism

3.4.1 The effect of PA6 crystal structure and crystallinity

Since the crystal structure and crystallinity of polymer will contribute, at certain degree, to the change of impact strength.^{22, 49-52} So we carried out DSC experiment to investigate crystal structure and crystallinity of the different samples. The first melting curves of the PHE1 and PHE2 blends samples were shown in Fig. 7. Only one melting peak around 220 °C was seen for each sample, which corresponding to the melting of α phase. Hence, the change of the impact strength of samples is not caused by the change of crystal structure. The crystallinity is calculated from the equation :

$$\text{Crystallinity} = \frac{\Delta H_f}{\Delta H_f^m \chi_A} \times 100\% \quad (1)$$

where ΔH_f is the enthalpy of PA6 for the blends, ΔH_f^m is the enthalpy of PA6 whose crystallinity is 100%, the literature value 190 J/g is used (α phase).⁴⁰ χ_A is the content of PA6 for the blends.

Fig. 8 shows the crystallinity and melting point of the EPDM1 and EPDM2 system samples. The PA6 crystallinity in all ternary blends was at a constant level of 30%, and the PA6 melting point was almost 221 °C which indicates that annealing has no effect on the inherent properties of PA6 phase. In the case of our ternary blend system, therefore, the difference in the PA6 crystallinity hardly accounted for the remarkable dependence of impact toughness on PA6/HDPE-g-MA/EPDM ternary blends. Moreover, the constant melting temperature indicates no degradation occurs during annealing for ternary blends.

3.4.2 The effect of particle size

From the fractured surfaces of the annealing samples shown in Fig. 3, it can be easily found that the size of dispersed phase increases gradually with annealing for PHE1 blends, and the notched Izod impact strength variation of the PHE1 blends as a function of core-shell particles size (d_n) was plotted and shown in Fig. 9. Very interestingly, the impact strength exhibits a monotonous decrease with the increase of core-shell particles size from 0.49 μm to 0.91 μm , indicating an optimum particle size range (about 0.5 μm) was identified for annealed PHE1 blends. According to the Paul, DR et al research,⁵³⁻⁵⁵ the optimum particle size range of rubber toughened semicrystalline PA6 is 0.2-0.5 μm . Therefore, it can be concluded that the curve in Fig. 9 is only the ductile-brittle transition region and this optimum particle size for our toughened PA6 seems reasonable.

For PHE2 system, the size of dispersed phase fluctuated around 0.5 μm calculated from Fig. 3e-f, which indicated that the changed impact strength is not caused by the effect of dispersed phase particle size.

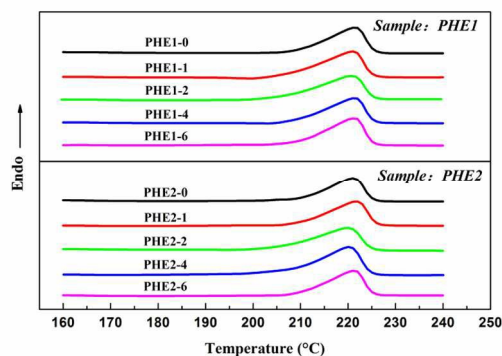


Fig. 7 DSC melting curves of different samples

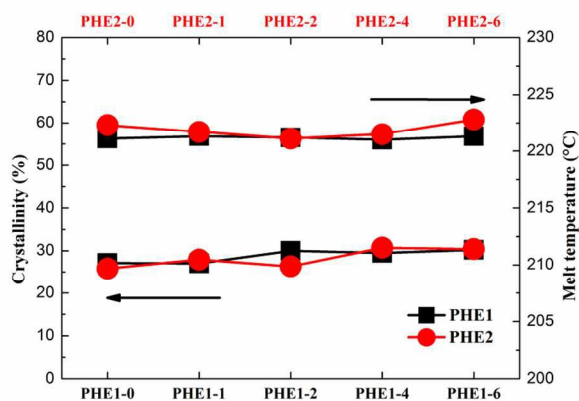


Fig. 8 The crystallinity and the melting point of different samples.

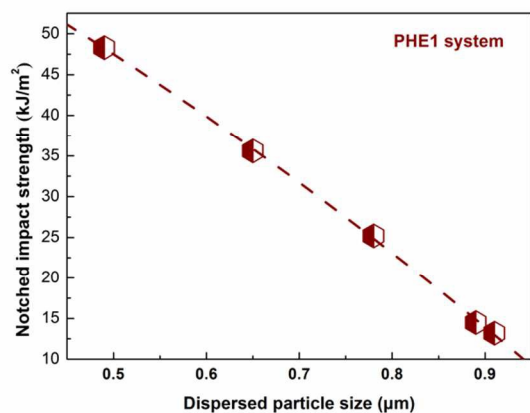


Fig. 9 Impact strength of PHE1 blends as a function of number-average particles diameter (d_n).

3.4.3 Crack initiation patterns in crack tip

The OM micrographs from the crack-initiation region of the unbroken notches pure PA6 and PA6/HDPE-g-MA/EPDM blends with PHE1-0, PHE1-6, PHE2-0 and PHE2-6 as examples are shown in Fig. 10. Two important factors should be considered as regards these OM images: (i) the darkness size of damage zone corresponding to the extent of craze growth and (ii) the darkness degree of the damage zone which represents the intensity and number of crazes.⁵⁶ If a polymer system can generate a massive number of crazes during deformation, then a tough polymer may result. On the other hand, crazes could also lead to early and low-energy failure of polymers when only a small density of crazes is generated; in this case the polymer would fail in a brittle manner due to the premature breakdown of a few crazes. It can be found that no obvious microcraze spreads into the matrix in the crack tip region for PA6 (shown in Fig. 10(a1)) and the area of crack region is only $23.1 \mu\text{m}^2$, indicating a brittle behavior was observed. For PHE1-0 and PHE1-6, there are obvious differences of fracture mechanism. Compare with a larger damage region for PHE1-0 with area of 0.97 mm^2 , more serious crack propagation and more obvious cracks can be noticed for PHE1-6 sample, implying inferior effect of preventing crack propagation. Also the area of damage region for PHE1-6 is 0.52 mm^2 which is in accord with its lower impact strength. In comparison, large yield-region can be both seen for PHE2-0 and PHE2-6 and the area of crack region is 1.2 mm^2 and 0.95 mm^2 which is larger than that of PHE1 system respectively. However, it should be note that no sign of massive crack propagation is observed in the edge of yield-region for PHE2-0, which is well consistent with the high

notch impact strength. In addition, plastic deformation around the craze could also be evidenced by the presence of a birefringent zone in PHE1-0, PHE2-0 and PHE2-6 (Fig. 10 (b2), (d2) and (e2)), indicating that shear-yielding mechanism occurs along the crack trigger. These damage features are also observed in toughened PP blends.⁵⁷⁻⁵⁹

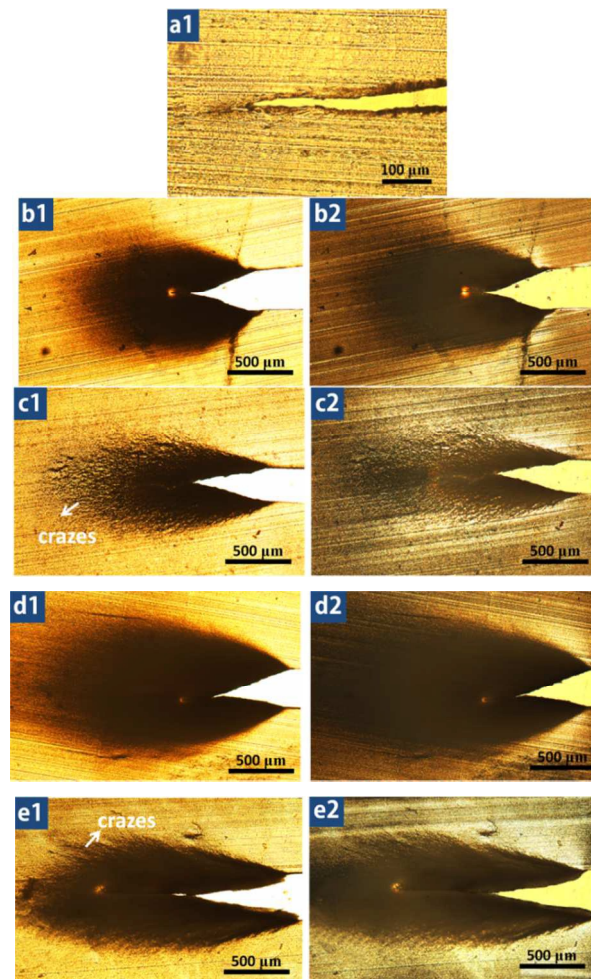


Fig. 10 Crack initiation patterns of the samples after the Izod notched part-impact test. (a) pure PA6, (b) PHE1-0, (c) PHE1-6, (d) PHE2-0, (e) PHE2-6. The subscripts "1" and "2" represent bright field OM and cross polarized field OM, respectively.

3.4.4 The investigation of impact fracture

The dependence of impact strength and particle size for PHE1 system was shown in Fig. 9. Even so, the detailed toughening mechanism by the core-shell particles still remains unclear. To understand the fracture and toughening mechanism well, morphological features of the impact fractured surfaces are checked, and the corresponding results are collected in Fig. 11. At a glance, it appears largely difference for the blends with different core-shell dispersed particles. Clearly, many homogeneously distributed thick and long strips and intensive plastic deformation (shear yielding) are observed in Fig. 11a. This seems like the shear yielding mechanism and is possibly attributed to the optimum particle size ($d_n=0.49 \mu\text{m}$). Fig. 11b shows a flat fracture surface without visible plastic deformation which means that the dispersed particles activated shear yielding of PA6 matrix scarcely occurs in the PHE1-6 blends. Additionally, debonding is distinct in the PHE1-6 sample due to the weak interfacial adhesion caused by the coarsened dispersed

particles, which is consistent with its lowest impact strength (13.2 kJ/m^2). In comparison of the observation for PHE1-0 shown in Fig. 11a, similar toughened fracture morphology of PHE2-0 can be seen in Fig. 11c. However, a close inspection reveals a higher density of the yield strips in the PHE2-0 blends, which of that is lower for PHE1-0 blends, indicating more effective termination effect of crack propagation, which is consistent with its highest impact strength (64.9 kJ/m^2). Fig. 11d reveals the presence of voids and slight local matrix plastic deformation across the fracture surface in the PHE2-6 blend. The formation of voids and deformation corresponds to the pull-out and fibrillation of dispersed core-shell particles during impact tests. Thus, it is expected that some extent of plastic deformation occurs within ductile EPDM/HDPE-g-MA core-shell particles even pulled out from the matrix due to good interfacial adhesion in the PHE2-6 blends, which is essentially different from the debonding of the coarsened dispersed particles in the PHE1-6 blends with negligible interfacial adhesion. Therefore, combining with the morphological evolution of PHE2 blends (shown in Fig. 3), it can be concluded that the above fracture behavior for PHE2 blends is markedly affected by the changed core-shell type.

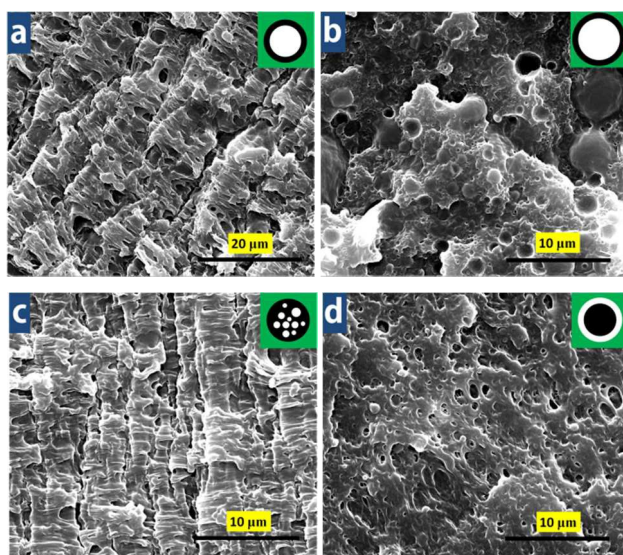


Fig. 11 Impact fracture morphology of different samples: (a) PHE1-0, (b) PHE1-6, (c) PHE2-0 and (d) PHE2-6. (In the sketch map, the green color represents PA6 phase, the white color represents HDPE-g-MA phase and the black color represents EPDM1 or EPDM2.)

3.4.5 The investigation of cross-section underneath the impact-fractured surfaces

More microstructure information can be further confirmed by observing the cross sections underneath the impact fractured surfaces.^{12, 16, 57} The observation position of samples is shown in Fig. 12. Away from the fracture surface, the severity of the plastic deformation changed because of the different phase structure, as shown in Fig. 13. Overlarge voids and naked/debonding fiber or spherical dispersed particles can be observed under the fracture surface of PHE1-0 in the enlarge image of Fig. 13a, and the voids seem to be lined up, indicating that the voids are initiated within the fibrillar dispersed particles, while smooth surface without any plastic deformation can be observed for PHE1-6 (Fig. 13b). In comparison, in the PHE2-0 blends, massive plastic deformation and large-area fibrillation can be seen, and no sign of naked/debonding spherical particles can be noticed (Fig. 13c). Additionally, large amount of microvoids emerge in the cross section of PHE2-6 (Fig. 13d) which may attribute to its core-shell structure inability. These observations

are consistent with the impact properties.

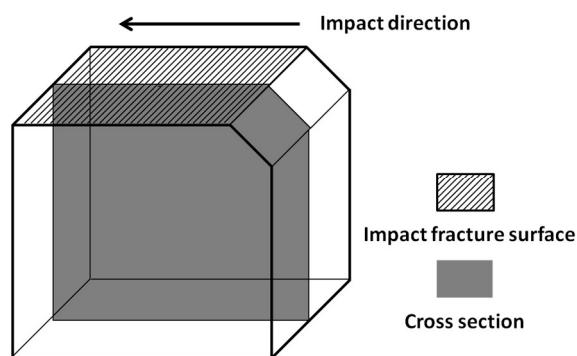


Fig. 12 Schematic of the core cross-section of a broken Izod impact bar for SEM observations.

3.5 The relation of structure and property

It is generally accepted that microvoiding is the essential step which triggers matrix shear yielding, thereby resulting in considerable energy dissipation.⁶⁰⁻⁶² Microvoiding can occur either by internal cavitation or debonding.⁶³⁻⁶⁵ After clearly observation of Fig. 13a and c, the formation mechanism of microvoids for PHE1-0 and PHE2-0 can be attributed to debonding and internal cavitation, respectively. Moreover, the size of the microvoids in the PHE1-0 blends is rather smaller than that of PHE2-0.

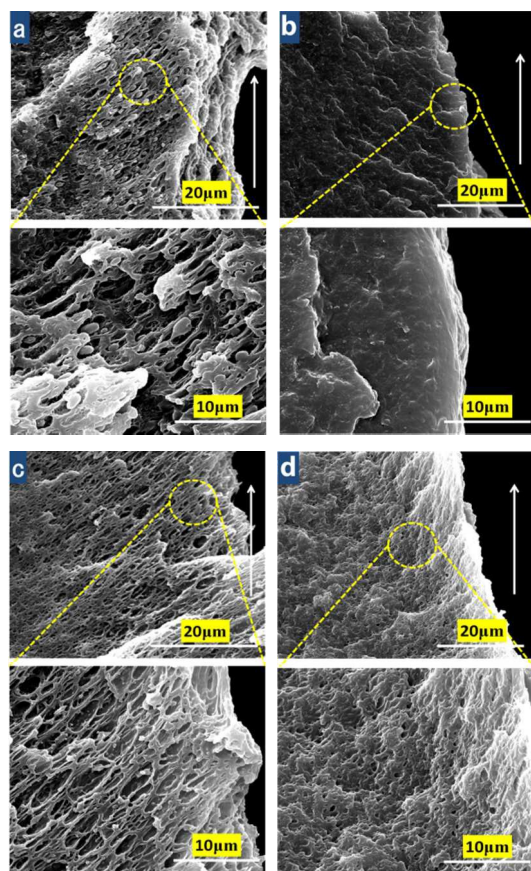


Fig. 13 SEM micrographs of cross sections underneath the impact-fractured surfaces. (a) PHE1-0, (b) PHE1-6, (c) PHE2-0, (d) PHE2-6. The bottom photos are the high magnification of the yellow circle for the counterparts. The white arrow represents the crack-propagation direction.

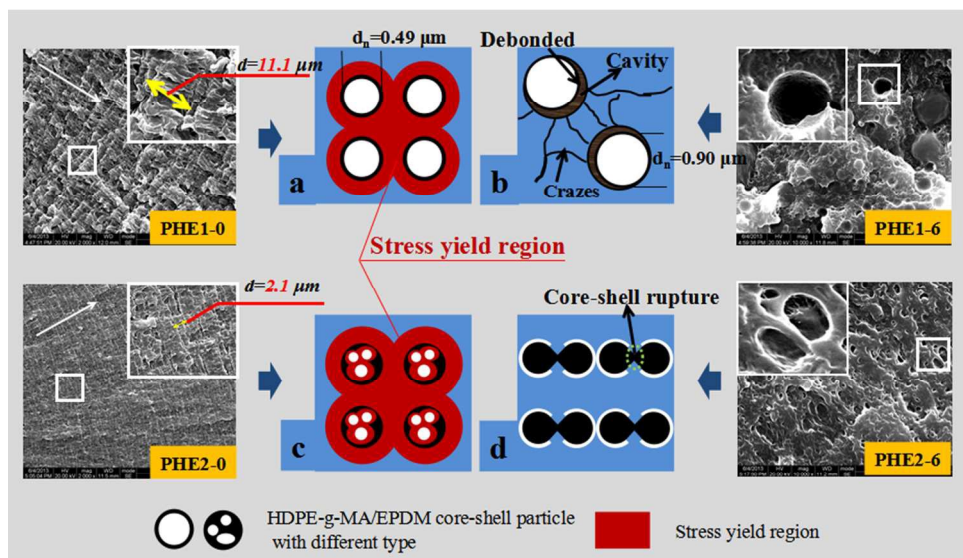


Fig. 14 A sketch showing the toughening mechanism changes for different morphologies. (a) PHE1-0, (b) PHE1-6, (c) PHE2-0, (d) PHE2-6. The white arrow represents the crack-propagation direction

Fig. 14 shows a sketch for the toughening mechanism changes of PA6/HDPE-g-MA/EPDM blends in different morphologies. As is clearly observed in **Fig. 14a**, due to the smaller size of core-shell particles ($d_n=0.49\mu\text{m}$), the stress fields around particles seem to serve as a bridge between two neighboring core-shell particles and the stress yield around individual particle would interfere with each other resulting the matrix yielding would propagate and pervade over the entire matrix, and then the blend would be tough. In contrast, for the PHE1-6 blend, because average core-shell particle size increases to $0.90\mu\text{m}$, which makes it far out of optimum particle size ($d_n=0.2\text{--}0.5\mu\text{m}$) for toughening PA6. It has been reported by numerous researchers that only the size of the impact modifier particles exceeds a critical value the crazing of the matrix around them can be effectively initiated.^{20, 66, 67} But it should be noted that if the particles are too large, the cracks quickly passed through the weak interfaces and induced premature crack propagation due to the coalescence of crazes, following craze initiation and propagation at the early stage of the impact testing, and consequently, the impact specimens were unable to develop a substantial yield zone before the crack growth from the notch tip brought the test to an end, eventually giving the PHE1-6 blends inferior impact toughness.

For PHE2-0 with multi-core structure, large amount of HDPE-g-MA particles embed in the EPDM2 phase increases the interface area between HDPE-g-MA and EPDM which is larger than that for single-core structure in PHE1-0. Based on the relatively good miscibility of HDPE-g-MA and EPDM (shown in **Fig. 2b**), it can be concluded that multi-core structure with larger interface area has a higher strength than that for single-core structure. Also, HDPE-g-MA particles in the EPDM2 phase serving as “fillers” will enhance the multi-core structure strength synergistically. Then for PHE2-0, on one hand, an increase in the core-shell structure strength can bear a higher tensile stress during impact, avoid the rupture and debonding of multi-core particles and allow the expansion of the local plastic zone until the critical stress level is reached, causing large-area stress yielding of the matrix. On the other hand, the deformation of HDPE-g-MA particles could produce more micro-voids and then caused stress yielding. Meanwhile, the fibrotic HDPE-g-MA (shown in **Fig. 13c**) can absorb fracture energy and the enlarged interfacial area can prevent propagation of the crack. The SEM micrographs in **Fig.**

14 show that the thickness of shear strips for PHE2-0 ($d=2.1\mu\text{m}$) is smaller than that ($d=11.1\mu\text{m}$) for PHE1-0, indicating a higher density of strips on the same surface area, which is corresponding to better effect of crack propagation prevention. This is consistent with its highest impact strength. For PHE2-6, it should be pointed out that a reversing core-shell structure with HDPE-g-MA shell and EPDM core was achieved after annealing for the morphology of PHE2-6. **Fig. 14d** shows the fracture feature for PHE2-6. Due to the lower strength of EPDM2 compared with HDPE-g-MA, this type of core-shell particles maybe unstable during impact and could rupture when the critical stress level is reached, hence only cavitations can be found in the fracture surface without any sign of stress yielding, indicating lower impact strength.

Based on the above discussion, by considering that shear yielding is far more effective than crazing in energy dissipation, multi-core structure, formed during melt mixing, provides a deep understanding of elastomer toughened polymer blends. However, the effect of core number, size and properties on the performance of PA6 blends has not been widely investigated in this work which is not neglected. Further work is now being undertaken in our group.

IV. Conclusions

The hierarchical core-shell structure of PA6/HDPE-g-MA/EPDM ternary blends was successfully controlled using the quiescent melt annealing method. The effect of hierarchical core-shell structure evolution on the notch impact strength of the blends is tremendous, of which multi-core structure gives the blends much higher impact strength than other structures. The OM observation of crack-initiation region manifests that multi-core structure can not only effectively trigger massive micro-cracks, but can remarkably terminate the propagation of cracks. The correlation between particle size and impact toughness revealed that there existed an optimum particle size for PA6 toughening in this ternary blend system. It appeared that the crystallization of PA6 was not a contributing factor in achieving the super toughness in the ternary blends. The morphology of impact-fractured surface and cross sections underneath the impact-fractured surface indicate that multi-core structure with larger interface area and higher interfacial adhesion can bear a higher tensile stress during impact, avoid the rupture and debonding of multi-core particles and allow the expansion of the local plastic zone until the critical

stress level is reached, causing large-area stress yielding of the matrix. Moreover, the deformation of HDPE-g-MA particles can also produce more micro-voids to dissipate fracture impact energy and then gives higher impact strength.

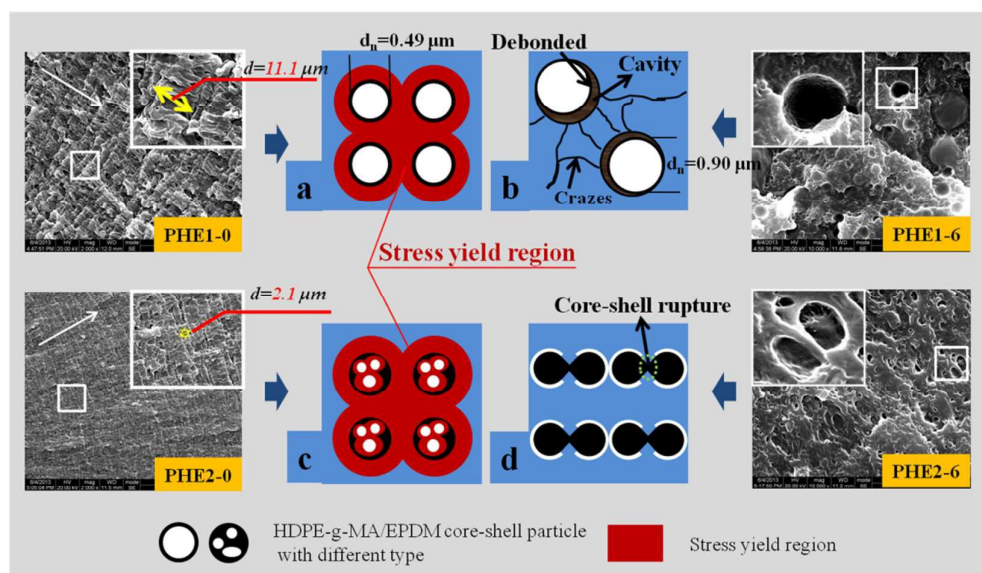
Acknowledgments

The authors gratefully acknowledge the financial support from the National Natural Science Foundation of China (Contract No. 51273219 and 5142106), the National Key Basic Research Program of China (973 Program, No. 2012CB025902), the Fundamental Research Funds for the Central Universities (No. 2013SCU04A03) and the Foundation of State Key Laboratory of Polymer Materials Engineering (Grant No. sklpm2014-3-12).

Notes and references

- D. R. Paul, J. W. Barlow and H. Keskkula, *Encyclopedia of polymer science and engineering*. New York: Wiley; 1988.
- R. A. Kudva, H. Keskkula and D. R. Paul, *Polymer*, 2000, **41**, 239-258.
- H. G. Fang, F. Jiang, Q. H. Wu, Y. S. Ding and Z. G. Wang, *ACS Appl. Mater. Interfaces.*, 2014, **6**, 13552-13563.
- M. L. Robertson, M. J. Paxton and M. A. Hillmyer, *ACS Appl. Mater. Interfaces.*, 2011, **3**, 3402-3410.
- D. Ponnamma, K. K. Sadasivuni, M. Strankowski, Q. P. Guo and S. Thomas, *Soft Matter*, 2013, **9**, 10343-10353.
- P. L. Corroller and B. D. Favis, *Polymer*, 2011, **52**, 3827-3834.
- S. Ravati and B. D. Favis, *Polymer*, 2010, **51**, 4547-4561.
- X. Q. Liu, R. H. Li, R. Y. Bao, W. R. Jiang, W. Yang, B. H. Xie and M. B. Yang, *Soft Matter*, 2014, **10**, 3587-3596.
- S. Ravati and B. D. Favis, *Polymer*, 2013, **54**, 3271-3281.
- L. P. Li, B. Yin, Y. Zhou, L. Gong, M. B. Yang, B. H. Xie and C. Chen, *Polymer*, 2012, **53**, 3043-3051.
- K. Wang, F. Chen, Z. M. Li and Q. Fu, *Prog. Polym. Sci.*, 2014, **39**, 891-920.
- J. P. Cao, X. D. Zhao, J. Zhao, J. W. Zha, G. H. Hu and Z. M. Dang, *ACS Appl. Mater. Interfaces.*, 2013, **5**, 6915-6924.
- R. Dou, W. Wang, Y. Zhou, L. P. Li, L. Gong, B. Yin and M. B. Yang, *J. Appl. Polym. Sci.*, 2013, **129**, 253-262.
- M. Umeda and I. Uchida, *Langmuir*, 2006, **22**, 4476-4479.
- K. Y. Zhang, A. K. Mohanty and M. Misra, *ACS Appl. Mater. Interfaces*, 2012, **4**, 3091-3101.
- Y. Lin, H. B. Chen, C. M. Chan and J. S. Wu, *Macromolecules*, 2008, **41**, 9204-9213.
- G. E. Molau and H. Keskkula, *J. Polym. Sci.*, 1966, **4**, 1595-1607.
- H. Z. Liu, L. Guo, X. J. Guo and J. W. Zhang, *Polymer*, 2012, **53**, 272-276.
- A. J. Oshinski, H. Keskkula and D. R. Paul, *Polymer*, 1992, **33**, 268-283.
- C. B. Bucknall and D. R. Paul, *Polymer*, 2009, **50**, 5539-5548.
- D. M. Laura, H. Keskkula, J. W. Barlow and D. R. Paul, *Polymer*, 2003, **44**, 3347-3361.
- J. J. Huang, H. Keskkula and D. R. Paul, *Polymer*, 2006, **47**, 639-651.
- Z. Ke, D. Shi, J. H. Yin, R. Li and Y. W. Mai, *Macromolecules*, 2008, **41**, 7264-7267.
- H. Yang, Q. Zhang, M. Guo, C. Wang, R. N. Du and Q. Fu, *Polymer*, 2006, **47**, 2106-2115.
- I. Luzinov, C. Pagnoulle and R. Jerome, *Polymer*, 2000, **41**, 7099-7109.
- S. Wu, *Polymer*, 1985, **26**, 1855-1863.
- K. Dijkstra and G. H. T. Bolscher, *J. Mater. Sci.*, 1994, **29**, 4286-4293.
- A. Lazzeri and C. B. Bucknall, *Polymer*, 1995, **36**, 2895-2902.
- P. A. Tzika, M. C. Boyce and D. M. Parks, *J. Mech. Phys. Solids.*, 2000, **48**, 1893-1929.
- R. J. M. Borggreve, R. J. Gaymans, J. Schuijjer and J. F. I. Housz, *Polymer*, 1987, **28**, 1489-1496.
- van der Wal A and R. J. Gaymans, *Polymer*, 1999, **40**, 6067-6075.
- B. Yin, L. P. Li, Y. Zhou, L. Gong, M. B. Yang and B. H. Xie, *Polymer*, 2013, **54**, 1938-1947.
- N. R. Demarquette, A. M. C. Souza, G. Palmer and P. H. P. Macaubas, *Polym. Eng. Sci.*, 2003, **43**, 670-683.
- S. Wu, *Polymer interface and adhesion*. New York: Marcel Dekker, 1982.
- H. Gramespacher and J. Meissner, *J. Rheol.*, 1992, **36**, 1127-1141.
- A. M. C. Souza and N. R. Demarquette, *Polymer*, 2002, **43**, 1313-1321.
- A. M. C. Souza and N. R. Demarquette, *Polymer*, 2002, **43**, 3959-3967.
- P. H. P. Macaubas and N. R. Demarquette, *Polymer*, 2001, **42**, 2543-2554.
- S. A. Saltikov, *Proceedings of the second international congress for stereology*. Springer-Verlag: New York, 1967, p 163-173.
- I. Campoy, M. A. Gomez and C. Marco, *Polymer*, 1998, **39**, 6279-6288.
- J. Roeder, R. V. B. Oliveira, M. C. Goncalves, V. Soldi and A. T. N. Pires, *Polym. Test.*, 2002, **21**, 815-821.
- U. Sundararaj, C. W. Macosko and C. K. Shih, *Polym. Eng. Sci.*, 1996, **36**, 1769-1781.
- U. Sundararaj, *Macromol. Symp.*, 1996, **112**, 85-89.
- J. Reignier and B. D. Favis, *AIChE. J.*, 2003, **49**, 1014-1023.
- P. L. Corroller and B. D. Favis, *Polymer*, 2011, **52**, 3827-3834.
- Y. Chen, Y. Chen, W. Chen and D. C. Yang, *Eur. Polym. J.*, 2007, **43**, 2999-3008.
- Ivan Fortelný, Josef Jůza, Tařana Vacková, Miroslav Šlouf, *Colloid. Polym. Sci.*, 2011, **289**, 1895-1903.
- L. Zhu, X. H. Xu and J. Sheng, *J. Polym. Res.*, 2011, **18**, 1269-1275.
- O. K. Muratoglu, A. S. Argon, R. E. Cohen and M. Weinberg, *Polymer*, 1995, **36**, 921-930.
- J. J. Huang, H. Keskkula and D. R. Paul, *Polymer*, 2004, **45**, 4203-4215.
- J. J. Huang, H. Keskkula and D. R. Paul, *Polymer*, 2006, **47**, 624-638.
- J. J. Huang and D. R. Paul, *Polymer*, 2006, **47**, 3505-3519.
- A. J. Oshinski, H. Keskkula, D. R. Paul, *Polymer*, 1992, **33**, 268-283.
- A. J. Oshinski, H. Keskkula, D. R. Paul, *J. Appl. Polym. Sci.*, 1996, **61**, 623-640.
- A. J. Oshinski, H. Keskkula, D. R. Paul, *Polymer*, 1996, **37**, 4909-4918.
- A. Afshar, I. Massoumi, R. Lesan-Khosh and R. Bagheri, *Mater. Des.*, 2010, **31**, 802-807.
- C. Z. Geng, J. J. Su, S. J. Han, K. Wang and Q. Fu, *Polymer*, 2013, **54**, 3392-3401.
- F. Luo, J. Wang, H. Bai, K. Wang, H. Deng, Q. Zhang and Q. Fu, *Mater. Sci. Eng. A*, 2011, **528**, 7052-7059.
- A. Dasari, Q. X. Zhang, Z. Z. Yu and Y. W. Mai, *Macromolecules*, 2010, **43**, 5734-5739.
- A. F. Yee, D. M. Li and X. W. Li, *J. Mater. Sci.*, 1993, **28**, 6392-6398.
- G. M. Kim and G. H. Michler, *Polymer*, 1998, **39**, 5689-5697.
- G. M. Kim and G. H. Michler, *Polymer*, 1998, **39**, 5699-5703.
- R. J. M. Borggreve, R. J. Gaymans and H. M. Eichenwald, *Polymer*, 1989, **30**, 78-83.
- D. Dompas, G. Groeninckx, M. Isogawa, T. Hasegawa and M. Kadokura, *Polymer*, 1995, **36**, 437-441.
- H. J. Sue, J. Huang and A. F. Yee, *Polymer*, 1992, **33**, 4868-4871.
- E. Piorkowska, A. S. Argon and R. E. Cohen, *Macromolecules*, 1990, **23**, 3838-3848.
- S. Y. Hobbs, *Polym. Eng. Sci.*, 1986, **26**, 74-81.

Graphical abstract



Highlights

1. The hierarchical core-shell structure in PA6/HDPE-g-MA/EPDM ternary blend was firstly formed and controlled using simple melt mixing method.
2. A super toughness PA6 ternary blends with a multi-core structure (HDPE-g-MA subinclusions within EPDM phase) was obtained.